Environmental Science & Technology

pubs.acs.org/est

Article

Impacts of Soil NO_x Emission on O_3 Air Quality in Rural California

Tong Sha, Xiaoyan Ma,* Huanxin Zhang, Nathan Janechek, Yanyu Wang, Yi Wang, Lorena Castro García, G. Darrel Jenerette, and Jun Wang*

Cite This: Environ. Sci. Technol. 2021, 55, 7113−7122

Read Online

ACCESS | Metrics & More | Article Recommendations | Supporting Information

ABSTRACT: Nitrogen oxides (NO_x) are a key precursor in O_3 formation. Although stringent anthropogenic NO_x emission controls have been implemented since the early 2000s in the United States, several rural regions of California still suffer from O_3 pollution. Previous findings suggest that soils are a dominant source of NO_x emissions in California; however, a statewide assessment of the impacts of soil NO_x emission (SNO_x) on air quality is still lacking. Here we quantified the contribution of SNO_x to the NO_x budget and the effects of SNO_x on surface O_3 in California during summer by using WRF-Chem with an updated SNO_x scheme, the Berkeley Dalhousie Iowa Soil NO Parameterization (BDISNP). The model with BDISNP shows a better agreement with TROPOMI NO_2 columns, giving confidence in the SNO_x estimates. We estimate that 40.1% of the state's total NO_x emissions in July 2018 are from soils, and SNO_x could exceed anthropogenic sources over croplands, which accounts for 50.7% of NO_x emissions. Such considerable amounts of SNO_x enhance the monthly mean NO_2 columns by 34.7% (53.3%) and surface NO_2 concentrations by 176.5% (114.0%), leading to an additional 23.0% (23.2%) of surface O_3 concentration in California (cropland). Our results highlight the cobenefits of limiting SNO_x to help improve air quality and human health in rural California.

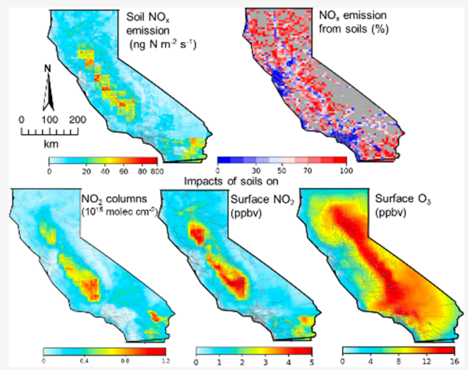

1. INTRODUCTION

Nitrogen oxides (NO_x = NO + NO_2) play a crucial role in tropospheric chemistry, which influence the oxidizing capacity of the troposphere by directly reacting with hydroxyl radicals (OH) and catalyzing the formation of ozone (O_3).[1] Most studies and regulatory policies in many countries, including the United States (U.S.), have focused largely on limiting anthropogenic NO_x emissions from motor vehicle and fossil fuel combustion. Previous studies have suggested soils as a significant source of NO_x emissions, accounting for one-fourth of the total global NO_x budget and even larger fractions over high-temperature fertilized agroecosystems and other dryland ecosystems following irrigation or precipitation events;[2−7] thus, SNO_x may have a contributing role in recent changes in air quality trends.

The U.S. Environmental Protection Agency (EPA) National Emission Inventory (NEI) reported a steady decrease in NO_x emissions from anthropogenic sources over the U.S. during the 2005−2018 period with a rate of 0.11 Tg N yr^{-1} or 54% overall.[8] However, the trend of tropospheric NO_2 column densities (columns) observed by satellites and nationwide NO_2 concentrations predicted by an ensemble of models are both inconsistent with the sustained decrease in NO_x emissions reported by the NEI, which stopped decreasing after the year of 2009.[9,10] Silvern et al.[11] separated OMI observations into winter and summer as well as urban and rural and found that OMI NO_2 in rural summer during the 2005−2017 period had no significant reduction trend. Furthermore, an increase in daily nonpeak O_3 concentration was observed in many parts of the U.S.[12−15] Recent studies suggest that this enhancement of O_3 can be mainly attributed to the temperature-driven increase in NO_x emission, mostly from soils.[2,16] Consequently, soils may be an important source of NO_x that has been overlooked in previous studies and regulatory frameworks but has a potentially increased impact on tropospheric NO_x budget and O_3 pollution.

Regional air quality models are often used to investigate the impact of emission sources on air quality and evaluate the effectiveness of emission control strategies.[17−20] SNO_x varies nonlinearly with region-specific agricultural management, soil conditions, and meteorology and in drylands may predominantly be emitted as a pulsed flux in response to irrigation/precipitation-drying cycles;[5,21,22] however, these relationships are not well constrained in models. Most models predict SNO_x as a function of surface air temperature, soil moisture, and ecosystem type, such as the Yienger and Levy model (YL95),[23] or the Model of Emissions of Gases and Aerosols from Nature (MEGAN, the scheme widely used in WRF-Chem),[24,25] which generally underestimates SNO_x fluxes and neglects the

Received: October 10, 2020
Revised: January 12, 2021
Accepted: February 2, 2021
Published: February 12, 2021

irrigation/precipitation-induced emission pulses from dry soils. Oikawa et al.[2] found that SNO_x calculated by MEGAN in WRF-Chem was underestimated by a factor of 10 in comparison to NO_x chamber measurements in rural California. Many studies have reached an agreement that numerical models generally underestimate SNO_x and misrepresent some key spatial and temporal features, which could be attributed to several uncertainties in the model settings, such as inaccurate emissions coefficients, poor soil moisture data, derivation of soil temperatures from surface air temperatures, neglect of nitrogen deposition, and lack of inclusion of emission pulses.[4,6,21,26−28]

We address the uncertainty in the role of SNO_x on regional-scale atmospheric chemistry through a combination of new satellite observations of tropospheric NO_2 distributions (TROPOMI) and revision of an SNO_x scheme that is subsequently added in the WRF-Chem model. The default SNO_x scheme in WRF-Chem, MEGAN v2.04, was replaced by adding the Berkeley Dalhousie Soil NO Parameterization (BDSNP) scheme with modifications to better represent land cover distributions, soil temperature representation, and emission pulses, as well as include fertilizer N emissions from agricultural soils (hereafter the Berkeley−Dalhousie−Iowa Soil NO parameterization or BDISNP). Within the U.S., the state of California has the highest agricultural output, as well as extensive agricultural and natural drylands. In croplands, where nitrogen-rich fertilizers are applied to soils and have regular irrigation, NO_x emissions can be significantly enhanced in comparison to the urban regions.[29] Additionally, California has been experiencing warmer temperatures and increasing droughts.[30,31] Some rural regions, such as the Imperial Valley, San Joaquin Valley, and South Coast, also suffer from O_3 pollution that regularly exceeds government standards.[2,15] We thus choose California as a case study region and predict that SNO_x could contribute to both NO_x and O_3 distributions in the atmosphere. Our results provide insights needed for developing more effective emission reduction strategies to improve the air quality of California and other regions, especially in rural areas with a high prevalence of respiratory illnesses.

2. MATERIALS AND METHODS

2.1. Model Configurations. The Weather Research and Forecasting (WRF) model coupled with online chemistry (WRF-Chem) version 3.8.1 was used in this study.[32] The simulation was performed on one domain over the western U.S. with a grid spacing of 12 km and 74 vertical levels. The physical schemes include the Morrison 2-moment microphysical scheme, Grell 3-D cumulus scheme,[33] RRTM for longwave radiation,[34] and Goddard scheme for shortwave radiation,[35] Yonsei University planetary boundary layer scheme,[36] and Noah land surface model.[37] The Regional Acid Deposition Model, Version 2 (RADM2) for gas-phase chemistry,[38] the Modal Aerosol Dynamics Model for Europe (MADE)[39] and the Secondary Organic Aerosol Model (SORGAM) aerosol modules with some aqueous reactions were chosen.[40]

The 0.625° × 0.5° Modern-Era Retrospective analysis for Research and Applications, Version 2 (MERRA-2) reanalysis data provide the meteorological initial and boundary conditions.[41] MERRA-2 is produced using the Goddard Earth Observing System (GEOS) atmospheric data assimilation system and uses observations to correct the model simulated precipitation over tropical and midlatitude land areas (60°S−60°N).[42] The 0.25° × 0.25° Global Land Data Assimilation System (GLDAS) data provides the initial and boundary conditions of soil properties (e.g., soil moisture and temperature).[43] Anthropogenic emissions were imported from the U.S. EPA NEI in 2011. Biomass burning emissions are from Fire Locating and Modeling of Burning Emissions Inventory (FLAMBE).[44−46] The simulation was conducted from 29 June to 31 July 2018 with the first 2 days as the spin-up period. The model output from 1 July to 31 July was analyzed.

2.2. Implementation of BDISNP in WRF-Chem. The BDISNP scheme is based on the BDSNP scheme[4] with a few changes to improve its adaptation to WRF-Chem. Within the BDISNP, the base emission coefficient is composed of two parts: one is the biome emission factor depending on 20 MODIS land cover types, and the other is the available nitrogen in soils including fertilizer and deposition N, which is also used to adjust the base emission coefficients for each biome. It also considers the nonlinear change of SNO_x flux with multiple environmental and meteorological factors including soil temperature, soil moisture, the precipitation-induced emission pulse from dry soils, and canopy effects. The function of SNO_x flux (detailed in SIs) can be expressed as

$$F_{SNO_x} = A_b'(N_{\mathrm{biome}} + N_{\mathrm{avail}}) \times f(T) \times g(\theta) \times P(l_{\mathrm{dry}}) \times (1 - \mathrm{CRF}) \quad (1)$$

where F_{SNO_x} (mol km^{-2} h^{-1}) is the SNO_x flux, A_b' is the base emission coefficient, and N_{biome} (kg N m^{-2} s^{-1}) and N_{avail} (kg N m^{-2} s^{-1}) are the wet/dry biome emission factor and nitrogen source availability in soils, respectively. The adjusting factors include soil temperature and moisture factor ($f(T)$, $g(\theta)$), pulsing factor ($P(l_{\mathrm{dry}})$), and canopy reduction factor (CRF). T (°C) and θ (unitless) are the soil temperature and water-filled pore space (WFPS, defined as the ratio of the volumetric soil moisture content to the porosity), respectively. l_{dry} (h) is the length of the dry period, which is determined by the variation of soil moisture rather than the amount of precipitation.

As one of the important input data of the SNO_x scheme, the N fertilizer emissions account for the timing and distribution of N fertilizer on the basis of the MODIS-derived seasonality of the canopy. Since the total N fertilizer use in 2017 in the U.S. (11649324 tons; the data in 2018 are not available, http://www.fao.org/faostat/en/#data/RFN) is similar to that in 2006 (11625400 ton in U.S., the baseline year of N fertilizer data used by Hudman et al.[4]) and California N fertilizer sales plateaued in the early 2000s,[47] we use the same fertilizer data from Hudman et al.[4] in the BDISNP.

In comparison to the BDSNP scheme, the BDISNP framework has three major modifications: (1) updating the default land cover data in the WRF model by using the Moderate Resolution Imaging Spectroradiometer Land Cover Type (MCD12Q1) Version 6 data (https://lpdaac.usgs.gov/products/mcd12q1v006/) in 2018 with a spatial resolution of 500 m to reproduce more a realistic biome type in BDISNP (Figure S1a,b), (2) using the GLDAS data to predict the initial and boundary condition of soil moisture and temperature and directly adopting the soil temperature at the top layer to simulate SNO_x rather than using 2 m air temperature (T2) as a proxy for soil temperature (e.g., soil temperature on dry soils

https://dx.doi.org/10.1021/acs.est.0c06834
Environ. Sci. Technol. 2021, 55, 7113−7122

with WFPS < 0.3 estimated as T2 + 5 °C at all times) in the BDSNP scheme, and (3) using the modeled green vegetation fraction (GVF) to determine the distribution of arid (GVF ≤ 30%) and nonarid (GVF > 30%) regions instead of using the static climate data as in the BDSNP scheme because the response of the soil moisture factor depends on climate zones and can vary by year.

2.3. Model Experiment Design. To show the improvement in model performance after updating the SNO_x scheme in WRF-Chem and evaluate the sensitivity of air quality to soil NO_x sources in rural California, we conducted four experiments: i.e., Default, BDSNP, BDISNP, and NoSNOx (Table 1). Default is the base simulation with the MEGAN scheme.

Table 1. Description of Model Experiments

experiment	description
Default	simulation uses MEGAN v2.04 to calculate soil NO_x emissions
BDSNP	simulation uses BDSNP to calculate soil NO_x emissions
BDISNP	simulation uses BDISNP to calculate soil NO_x emissions, including updates of land type to the year of 2018 and directly adoption of soil temperature at the top layer
NoSNOx	simulation is the same as BDISNP except that the NO_x emissions from soils are turned off

BDSNP is the simulation with the BDSNP scheme. BDISNP is the updated simulation with the BDISNP scheme, updated land types, and better soil temperature representation. NoSNOx is the same as BDISNP but without the soil NO_x emission.

2.4. Satellite-Based Observations. The TROPOMI (TROPOspheric Monitoring Instrument) instrument, aboard the European Space Agency (ESA) Sentinel-5 Precursor (S-5P) satellite, was launched on 13 October 2017. It provides almost daily global coverage of tropospheric column densities (denoted as columns) of NO_2 with an unprecedented horizontal spatial resolution of 3.5 × 7 km^2, has a better signal to noise ratio, and overpasses at about 13:30 local time (LT).[48,49] We use the level-2 daily gridded TROPOMI NO_2 data with quality controls: cloud-screened (cloud fraction below 30%) and quality-assured (qa_value above 0.50).[50] The averaging kernels (AK, defined as the altitude-dependent air mass factor) used in the retrieval algorithms are applied in the intercomparison between TROPOMI and WRF-Chem tropospheric NO_2 columns. Due to satellite data having irregular grid boxes, TROPOMI NO_2 was oversampled to the model grid (12 × 12 km^2).

The soil moisture observations were obtained from the Soil Moisture Active Passive Level 4 Soil Moisture (SMAP L4_SM) product, which merged lower-level SMAP data with the Goddard Earth Observing System-5 (GEOS-5) Catchment land surface model in the GEOS-5 ensemble-based land data assimilation system.[51] This product has a 9 × 9 km^2 horizontal resolution and is available twice daily (6:00 am and 6:00 pm LT).

Global Precipitation Measurement (GPM) provides observation data of precipitation every 3 h at a 0.25° × 0.25° spatial resolution. The Integrated Multi-satellitE Retrievals for GPM (IMERG) is the unified algorithm that provides rainfall estimates combining data from all passive-microwave instruments in the GPM Constellation.[52]

2.5. *In Situ* Measurements of NO_2 and O_3. Hourly surface NO_2 and O_3 measurements in California during July 2018 were obtained from the U.S. EPA Air Quality System (AQS) (https://www.epa.gov/aqs) to explore the implication of SNO_x to air quality. Seven NO_2 sites and 17 O_3 sites were selected to compare with the model simulations; the distribution of measurement sites is shown in Figure S1.

3. RESULTS AND DISCUSSION

3.1. Soil NO_x emissions. Figure 1b,c compares the distribution of simulated monthly mean SNO_x fluxes from

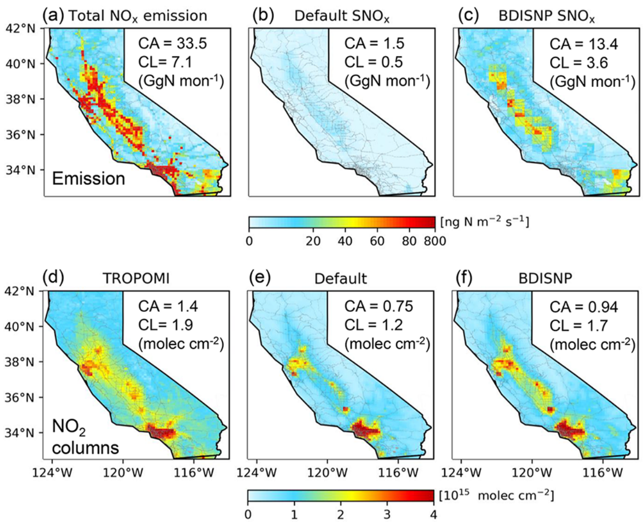

Figure 1. Distribution of the simulated monthly mean (a) NO_x emissions from all sources and SNO_x fluxes calculated by (b) Default and (c) BDISNP. (d) Monthly mean tropospheric NO_2 columns retrieved by TROPOMI measured at 12:00−14:00 LT and simulated by (e) Default and (f) BDISNP averaged over the same periods in July 2018. Statistics in the upper right corner of panels (a)−(c) are the monthly emissions averaged over the region of California (CA) and croplands (CL, shown as yellow land types in Figure S1b), respectively. Statistics in the upper right corner of panel (d-f) are the monthly mean NO_2 columns averaged over the region of California (CA) and cropland (CL), respectively. The gray dotted lines are roads in California.

the Default and BDISNP simulations. The implementation of the BDISNP scheme leads to SNO_x in July being 9 times higher than that of Default in California. The cropland regions (shown as yellow land types in Figure S1b), which include both high rates of fertilizer application and regular irrigation, show the largest SNO_x with monthly emissions of 3.6 Gg N mon^{-1} in BDISNP, while there is only 0.5 Gg N mon^{-1} in Default. Our results are consistent with those of Oikawa et al.,[2] which suggests that multiplying default soil NO_x emission rates in WRF-Chem by a factor of 10 can reach a level similar to the measurements of mean SNO_x in the Imperial Valley of California. The much greater SNO_x calculated by BDISNP reflects the improvements in the model that better reflect more diverse land covers, soil properties, agricultural management, and pulse emissions.

In comparison to BDSNP, BDISNP simulated monthly SNO_x in California decrease by 0.95 Gg N mon^{-1} (Figure S2). As the types of land covers in California have not changed much in the past 25 years (land cover types in Default are in 1993), only the area of certain land types has expanded or decreased. The higher SNO_x in BDSNP is mainly ascribed to its overestimation of soil temperature by assuming that the soil temperature is 5 °C higher than T2 for all land cover types on

https://dx.doi.org/10.1021/acs.est.0c06834
Environ. Sci. Technol. 2021, 55, 7113−7122

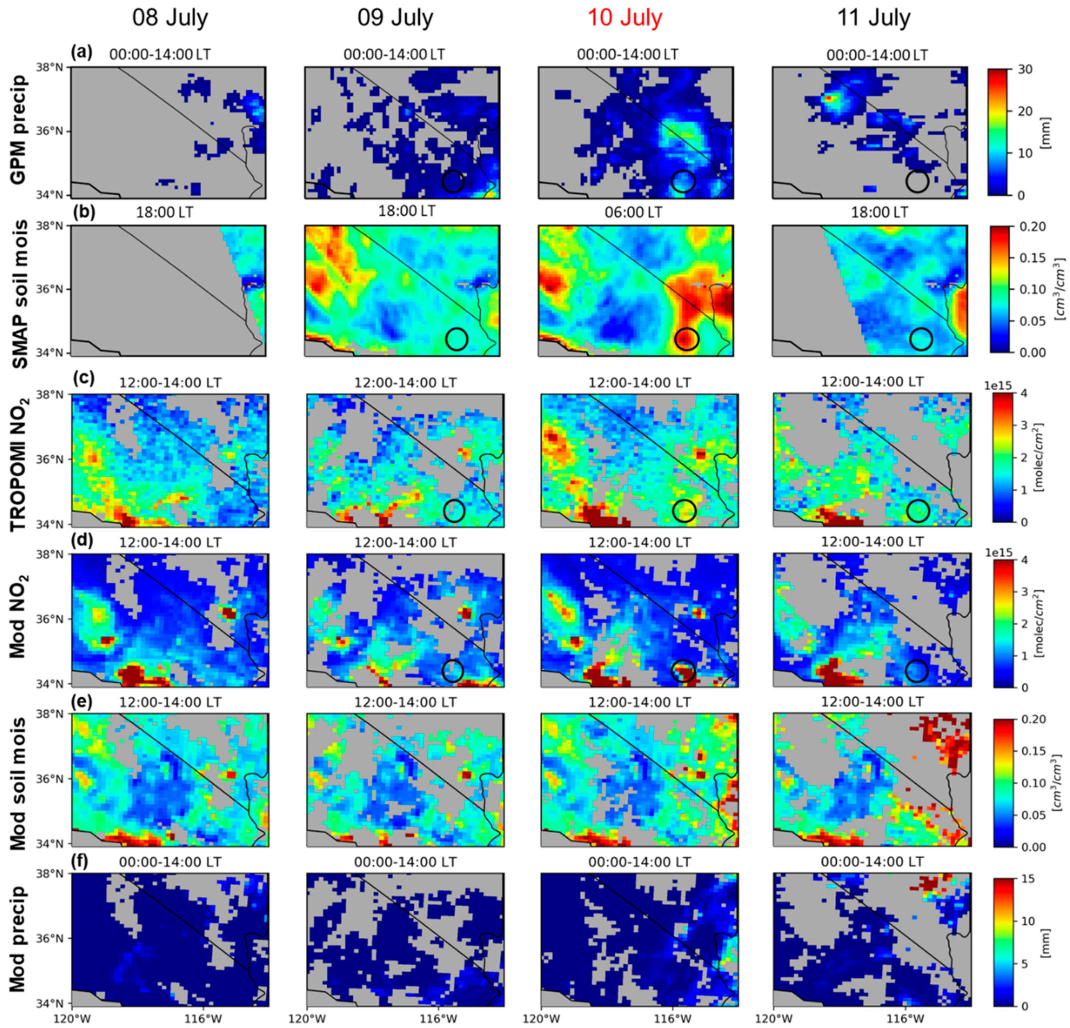

Figure 2. (a) Satellite-based distribution of the daily accumulated precipitation (00:00 to 14:00 LT prior to and during TROPOMI overpass time) from GPM rainfall product and (b) soil moisture from SMAP data in the rural area downwind from Los Angeles, California, during 8−11 July 2018. Also shown are distributions of daily tropospheric NO_2 columns from (c) TROPOMI and (d) BDISNP simulations, as well as distributions of (e) simulated soil moisture and (f) accumulated precipitation. The black circles denote the location of the Sheephole Valley, where we studied the SNO_x pulse event occurred on 10 July. A detailed georeferencing of Sheephole Valley is shown in Figure S1c.

dry soils (WFPS < 0.3) at all times. However, the WRF-Chem simulated daytime soil temperature is only on average 1 °C higher than T2 in California, and the difference between the soil and air temperature is much more dynamic than the constant 5 °C difference used in BDSNP (Figure S3). Indeed, the soil temperature in northern California covered with forests and savannas in average is 25.7 °C, 1.8 °C lower than T2, which in turn causes the soil temperature factor to increase from 14 (BDISNP) to 22 (BDSNP). Using T2 as a proxy for soil temperature in BDSNP can lead to large uncertainties in daily or hourly SNO_x estimation that are key to the hourly and daily O_3 prediction.

3.2. Tropospheric NO_2 Columns. Satellite-based observations of NO_2 have a wide spatial coverage in comparison to in situ measurements. TROPOMI with a finer spatial resolution is able to capture horizontal gradients and small-scale features, thus providing a good opportunity to evaluate the improvement of the BDISNP scheme in simulating NO_2 columns and detecting the NO_x emissions from soils. Here, we compare model simulations (Default and BDISNP) with TROPOMI NO_2 columns during July 2018 in California (Figure 1d−f). Default and BDISNP can reproduce the hot spots of NO_2 columns in urban regions shown in the TROPOMI NO_2 columns (e.g., San Francisco, Los Angeles), but both underestimate the monthly mean NO_2 columns to some extent by 1.4 (1.9) × 10^{15}, 0.75 (1.2) × 10^{15}, and 0.94(1.7) × 10^{15} molecules cm^{-2} for TROPOMI, Default, and BDISNP averaged over California (croplands), respectively. However, BDISNP shows improved performance in simulating tropospheric NO_2 columns in comparison to Default with a decreasing relative mean bias from 52.3% to 39.8% (Figure S4) and RMSE from 0.7 × 10^{15} to 0.6 × 10^{15} molecules cm^{-2} in California (Figure S5). The improvements over cropland are even more obvious; BDISNP reduces the mean bias and RMSE by nearly 23% and 38%, respectively, and increases the R value from 0.74 to 0.78, leading to a good agreement with the TROPOMI NO_2 columns (Figure S6).

Soil temperature is a major factor in the SNO_x scheme, and high-temperature fertilized soils can emit much higher NO_x levels.[2] We find that BDISNP can reproduce the observed response of daily NO_2 columns to temperature in rural areas but the Default could not (Figure S7). Although the

https://dx.doi.org/10.1021/acs.est.0c06834
Environ. Sci. Technol. 2021, 55, 7113−7122

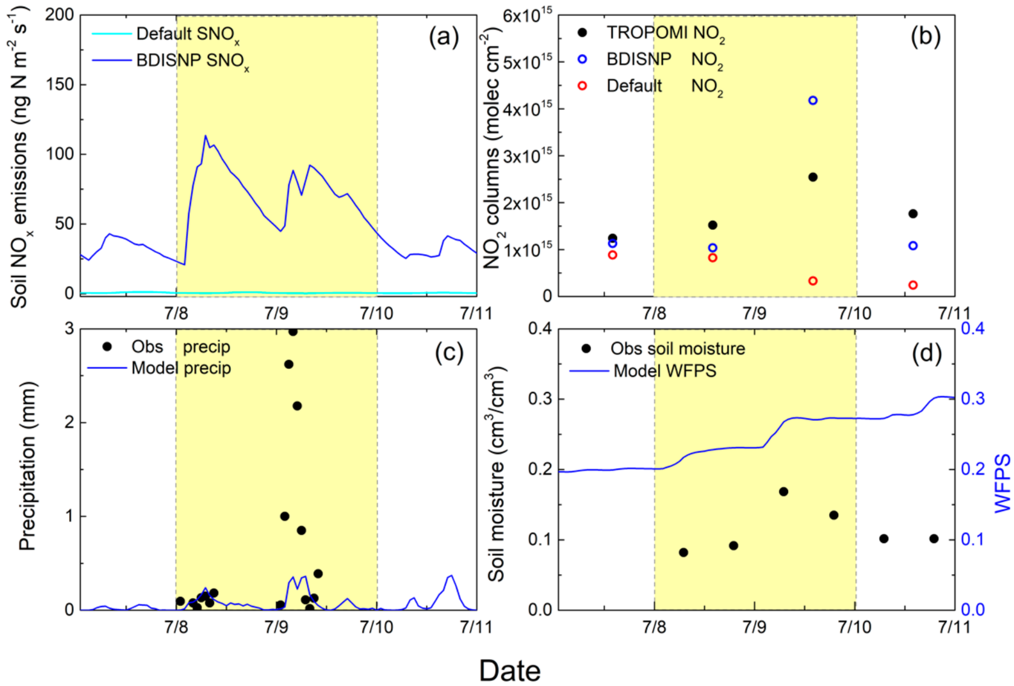

Figure 3. Time series of (a) simulated SNO_x fluxes calculated by Default and BDISNP, (b) tropospheric NO_2 columns from TROPOMI, Default, and BDISNP, (c) hourly precipitation from GPM observation and the BDISNP simulation, and (d) observed soil moisture from SMAP and simulated water-filled pore space (WFPS) from BDISNP over the Sheephole Valley during 8−11 July 2018.

instantaneous uncertainty of TROPOMI tropospheric NO_2 columns at the pixel level is 25−50% or can be up to 0.7×10^{15} molecules cm^{-2},[53] averaging over a larger area or for a longer time (such as 1 month) can largely reduce the noise and improve the precision of TROPOMIN NO_2 columns.[49,54] Therefore, in reference to the monthly TROPOMIN NO_2 columns, the improvement of NO_2 columns in BDISNP is credible, and the BDISNP scheme has the fidelity needed to study the implication of SNO_x to air quality in California.

We also investigate the impacts of SNO_x on tropospheric NO_2 columns in California, calculated as the difference between BDISNP and NoSNOx simulations (Figure S8). SNO_x causes the monthly mean NO_2 columns to increase by 0.2×10^{15} molecules cm^{-2} (34.7%) in California by following a distribution similar to that for modeled SNO_x. The largest impact is in croplands and drylands (shown as gray land types in Figure S1b, also called desert), where monthly mean NO_2 columns increase by 0.53×10^{15} molecules cm^{-2} (53.3%) and 0.31×10^{15} molecules cm^{-2} (57.2%), respectively.

3.3. Rain-Induced Emission Pulse. Pulsed SNO_x occurs when very dry soils are wetted by precipitation/irrigation, resulting in a reactivation of water-stressed bacteria, but most models do not consider this enhancement in SNO_x. The BDISNP scheme adopts the same approach of Hudman et al.,[4] in which pulsing activates once soils dry to a WFPS of 0.3 or less for at least three consecutive days prior to soil wetting. In this section, we evaluate the ability of the WRF-Chem model with the BDISNP scheme to characterize the pulsed emission in drylands: the Sheephole Valley of California (Figure S1c), which is in the Mojave Desert, experiences infrequent precipitation during the summer and is isolated from the urban NO_2 plumes. Due to the short photochemical lifetime of NO_x (<1 day) and high NO_2/NO_x ratio (>0.8) in the boundary layer, TROPOMI NO_2 with unprecedented resolution allows for SNO_x processes to be evaluated using observed NO_2 columns enhancements at spatiotemporal scales unresolvable with previous satellite-based NO_2 products.[29,55−57] Moreover, the contribution of lightning-generated and biomass-burning NO_x is shown to be minimal in Southern California in July 2018;[58−60] thus, the enhancement of TROPOMI NO_2 columns in the Sheephole Valley can therefore be mostly attributed to SNO_x.

We analyzed the multisatellite data with high temporal resolution, including daily TROPOMI NO_2 columns, 3 hourly GPM precipitation, and twice a day SMAP soil moisture observations and found that the observed precipitation was accompanied by the enhancement of soil moisture in the Sheephole Valley (the location of black circles in Figure 2a,b) on 10 July and there was no precipitation in this region before that date. Consequently, TROPOMI NO_2 columns increased on 10 July over the same region (Figure 2c). We hypothesize that this enhancement of NO_2 columns is due to the rain-induced NO_x emission pulse from dry soils.

As a test of the pulse emission hypothesis, we find that the BDISNP simulation can reproduce the enhancement of NO_2 columns and the pulsed emission from dry soils in the Sheephole Valley on 10 July (Figure 2d). The modeled peak SNO_x after the first precipitation can reach 114 ng N m^{-2} s^{-1} (Figure 3a), showing a similar level of peak NO_x flux postwetting in the Colorado Desert as measured by Eberwein et al. (the median value of ∼100 ng N m^{-2} s^{-1}).[22] These results suggest that the BDISNP scheme can characterize the rain-induced pulse, an improvement from the Default scheme. Such considerable SNO_x supported by both simulation results and field measurements in the Imperial Valley[2] and Colorado Desert[22] indicates that rural regions (including croplands and drylands) are major components of total NO_x emissions in California.

While a clear improvement against the Default simulation is found, the BDISNP-simulated NO_2 columns in the Sheephole

https://dx.doi.org/10.1021/acs.est.0c06834
Environ. Sci. Technol. 2021, 55, 7113−7122

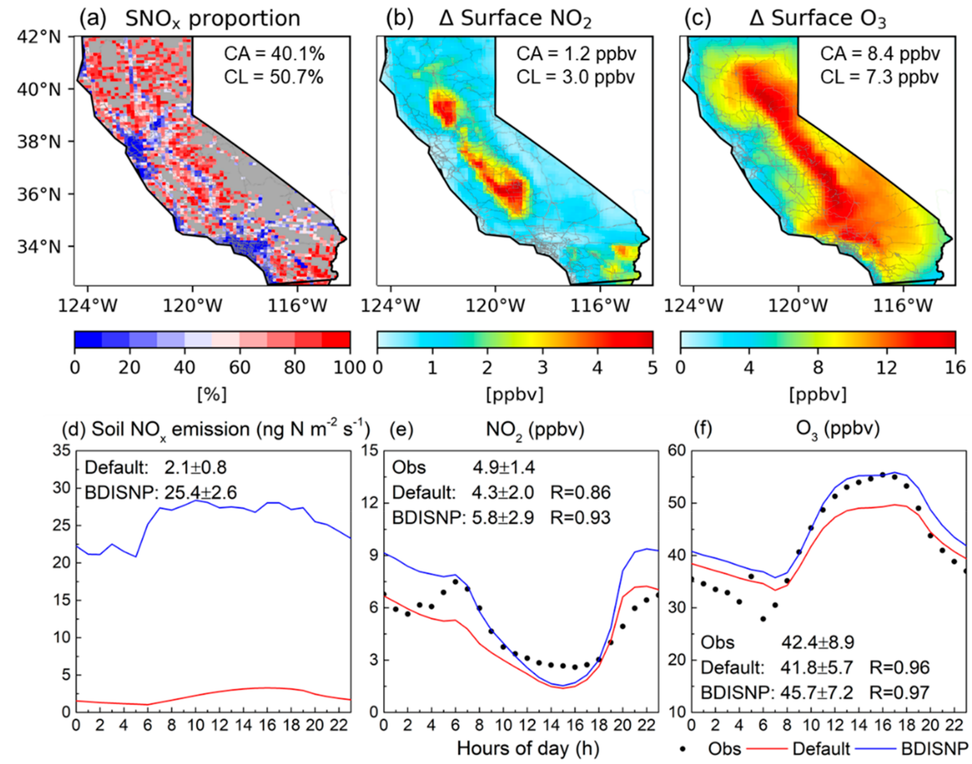

Figure 4. (a) Distribution of simulated contribution of SNO$_x$ to total NO$_x$ emissions. The grids where the monthly total anthropogenic NO$_x$ emissions are lower than 0.002 gN m^{-2} mon^{-1} are masked to better compare the relative importance of SNO$_x$ with anthropogenic sources. (b, c) Changes in surface NO$_2$ and O$_3$ concentration by the effects of SNO$_x$, calculated as the differences between BDISNP and NoSNOx simulations. Statistics in the upper right corner of (a)−(c) are the mean values averaged over the region of California (CA) and cropland (CL, shown as yellow land types in Figure S1b), respectively. The gray dotted lines are roads in California. Diurnal variations of (d) simulated SNO$_x$ fluxes, (e) surface NO$_2$, and (f) O$_3$ concentrations from the simulations (Default and BDISNP) and observations in the rural area downwind from Los Angeles, California, during July 2018. Statistics in (d) are the mean value ± standard bias. Statistics in (e) and (f) are the mean value ± standard bias and correlation coefficients between observations and simulations.

Valley on 10 July are 65% higher than that of TROPOMI (Figure 3b). This may be because the simulated precipitation began on 9 July, which caused the first NO$_x$ pulse in the Sheephole Valley after a long dry period. However, even with this precipitation, WFPS on July 9 is below 0.3 (soil moisture threshold to determine the timing of NO$_x$ pulsing). Hence, when the simulated precipitation still appeared on 10 July, the model simulates the second NO$_x$ pulse, causing the BDISNP to estimate greater emissions for multiple days and overestimate NO$_2$ columns on 10 July (Figure 3c,d). Huber et al.[29] suggested that a threshold of 0.3 for WFPS in BDSNP may overestimate emissions at lower soil moisture and underestimate emissions at higher soil moisture for some cropland soils. Therefore, the threshold of WFPS can be optimized further by comparing with ground-based measurements of NO$_x$ fluxes in future studies. Furthermore, the BDISNP-simulated precipitation and soil moisture have a certain bias in comparison with the observations. Accurate meteorological fields are critical to simulate the timing and distribution of SNO$_x$ when emissions are dominated by pulsing processes and require further study.

3.4. Impact of Soil NO$_x$ Emissions on Air Quality. With the implementation of BDISNP in WRF-Chem showing an improved simulation of atmospheric NO$_x$ distribution, we quantify the effects of SNO$_x$ on air quality in California. Figure 4 shows the proportion of SNO$_x$ to total NO$_x$ emissions in July and the change in monthly mean surface NO$_2$ and O$_3$ concentrations due to the effects of SNO$_x$, calculated as the amount of differences between BDISNP and NoSNOx simulations. We found that the substantial NO$_x$ emissions from soils in California, a previously overlooked source, can contribute to 40.1% of the state's total NO$_x$ budget (Figure 4a). Over croplands with high fertilizer application, such as the Central Valley and Imperial Valley, the NO$_x$ from soils rivals anthropogenic contributions, which account for 50.7%. A larger proportion of SNO$_x$ is found over drylands in Southern California in comparison to croplands, suggesting that wetting dry desert soils after precipitation to produce large emission pulses could cause SNO$_x$ to exceed anthropogenic sources, accounting for 76.1%. Our results are consistent with a prior study on SNO$_x$ estimates by using bottom-up models and spatially and temporally limited airborne measurements,[61] suggesting that agricultural soils could contribute to 20−51% of California's total NO$_x$ emissions. Such large amounts of NO$_x$ emissions from soils have significant impacts on air quality, which increase the monthly mean surface NO$_2$ concentrations by 1.2 ppbv (176.5%) in California, 3.0 ppbv (114.0%) in croplands, and 1.1 ppbv (183.8%) in drylands. The monthly mean surface O$_3$ concentrations also increase by up to 8.4 ppbv (23.0%) in California, 7.3 ppbv (23.2%) in croplands, and 9.5 ppbv (24.8%) in drylands (Figure 4b,c and Figure S9).

On consideration that SNO$_x$ has such a large influence on surface NO$_2$ and O$_3$ concentrations in rural California, we compared the diurnal variation of modeled NO$_2$ and O$_3$ with EPA observations over the downwind area of Los Angeles (the

https://dx.doi.org/10.1021/acs.est.0c06834
Environ. Sci. Technol. 2021, 55, 7113−7122

pink rectangle in Figure S1d), which has a high air temperature (>40 °C) during the summer. The simulated SNO_x fluxes calculated by BDISNP and Default are also shown in Figure 4. It is seen that the implementation of the BDISNP scheme leads to an SNO_x flux 12 times higher than that of the Default in this rural region, with the peak occurring in the daytime. BDISNP with the elevated SNO_x flux significantly increases the surface NO_2 concentrations in the early morning and predicts a diurnal variation similar to the observation (R values for the diurnal variations of 0.86 and 0.93 in Default and BDISNP, respectively). Within the Default scheme, the model underestimates O_3 concentrations in the daytime and estimates average monthly O_3 at 41.8 ppbv in this region. However, the BDISNP scheme increases surface O_3 concentrations by 9.3% (3.9 ppbv) and shows a better agreement with the observed diurnal variation. These results suggest that the atmospheric chemistry in this rural region is NO_x-limited and the air quality is sensitive to SNO_x. Therefore, the intensive agricultural practices and dry desert soils associated with high SNO_x in rural regions likely contribute to poor air quality in California by elevating O_3 concentrations.

Nevertheless, even after the SNO_x scheme in WRF-Chem is updated, the simulated tropospheric NO_2 columns and surface NO_2 concentrations in the afternoon are still lower than those observed. There are a few factors that could lead to model underestimations, including the uncertainties in the SNO_x scheme, underestimations of NO_x emissions from other sources, deviations of simulated meteorological fields, and TROPOMI retrieval errors.

For the SNO_x scheme, BDISNP assumes that NO_x emissions increase exponentially with soil temperature until the temperature reaches 30 °C. However, previous research suggested that SNO_x continues to increase with a nonlinear response to soil temperature when it is above 30 °C on the basis of NO_x chamber measurements in the Imperial Valley, California, and found that SNO_x can increase by 38% on average as the soil temperature increase from 30−35 °C to 35−40 °C.[2] It is thus necessary to improve the response of SNO_x in different land types to the soil temperature factor under high-temperature conditions. BDISNP also accounts for the loss of NO_x to the plant canopy on the basis of the work of Jacob and Bakwin.[62] However, its default canopy reduction scheme is not mechanistic in nature and may not accurately represent the temporal and spatial variability in canopy effects. We thus stress that future users of the model should implement a more appropriate canopy reduction scheme for their application, which can be achieved by using stomatal uptake to calculate the CRF through analyzing the laboratory measurements of stomatal NO_2 deposition to local vegetation.[63] In addition, the biome emission factors (e.g., grassland, savannas, and needleleaf) based on the work of Steinkamp and Lawrence[26] and the emission factor associated with fertilization (set to 2.5% in BDISNP) are uncertain and may be underestimated. Consequently, a more intensive evaluation of the BDISNP scheme is needed when ground-based measurements of NO_x flux are available to improve the parameterization in future studies.

Underestimating NO_x sources from anthropogenic emissions, lightning, and biomass burning can also account for the discrepancies. Furthermore, the EPA NEI used in this study is from 2011, which is believed to have an overestimation of NO_x emission by up to a factor of 2 in summer months.[64−67] Although lightning is rare[58−60] and there were no large fire activities occurring in July 2018 in California (https://worldview.earthdata.nasa.gov/), nevertheless the uncertainty of NO_x emissions from lightning and the lack of biomass burning in the model may thus lead to underestimating tropospheric NO_2 columns. SNO_x is also dependent on accurate meteorological fields in the model; a mischaracterized meteorology therefore could lead to these discrepancies. Additionally, because surface variables, such as soil moisture and temperature, are dependent on land cover types and are highly sensitive to the choice of land surface models,[68] updating land cover types and improving the performance of the land surface model in the future can better simulate SNO_x fluxes. On the other side, the KNMI-DOMINO product determines the stratospheric portion of NO_2 columns by assimilating slant columns in the TM5-MP chemistry transport model, but the stratospheric NO_2 columns can be lower than ground-based measurements by up to 0.15×10^{15} molecules cm^{-2}.[69] The tropospheric averaging kernels archived in TROPOMI, which use NO_2 profile information coming from the chemistry transport model and data assimilation system to convert slant columns to vertical columns, could also have uncertainties. While the KNMI product is known to compare well with aircraft- and ground-based measurements of NO_2 columns,[70−72] these retrieval errors can nevertheless also lead to the discrepancies between model simulations and TROPOMI observations.

In summary, our results highlight that SNO_x is an important source of atmospheric NO_x in California, contributing ∼40% on a state average and more than 50% in rural regions (slightly larger than 50%) with high fertilizer application and in minimally managed native drylands. Therefore, soil NO_x emission should be included in regulations to reduce adverse effects to air quality and human health.

■ ASSOCIATED CONTENT

Supporting Information

The Supporting Information is available free of charge at https://pubs.acs.org/doi/10.1021/acs.est.0c06834.

> Overview of the BDISNP scheme, response of daily NO_2 columns to soil temperature, emission factors for 20 soil biomes, distribution of land cover types, location of the Sheephole Valley, and measurement sites of surface NO_2 and O_3, differences in simulated SNO_x flux between BDISNP and Default (BDSNP), frequency and distribution of the differences between soil and 2 m air temperatures, bias of simulated NO_2 columns in comparison to the TROPOMI, scatter plots of observed and simulated NO_2 columns in California, scatter plots of observed and simulated NO_2 columns in croplands, temporal variation of soil temperature and daily NO_2 columns, change in NO_2 columns by the effects of SNO_x, and distribution of simulated surface NO_2 and O_3 and relative changes in surface NO_2 and O_3 by the effects of SNO_x (PDF)

■ AUTHOR INFORMATION

Corresponding Authors

Jun Wang − *Department of Chemical and Biochemical Engineering, Center for Global and Regional Environmental Research, and Iowa Technology Institute, University of Iowa, Iowa City, Iowa 52242, United States;* orcid.org/0000-0002-7334-0490; Email: jun-wang-1@uiowa.edu

https://dx.doi.org/10.1021/acs.est.0c06834
Environ. Sci. Technol. 2021, 55, 7113−7122

Xiaoyan Ma – *Collaborative Innovation Center on Forecast and Evaluation of Meteorological Disasters (CIC-FEMD), Key Laboratory for Aerosol-Cloud-Precipitation of China Meteorological Administration, Nanjing University of Information Science & Technology, Nanjing 210044, People's Republic of China*; Email: xma@nuist.edu.cn

Authors

Tong Sha – *Collaborative Innovation Center on Forecast and Evaluation of Meteorological Disasters (CIC-FEMD), Key Laboratory for Aerosol-Cloud-Precipitation of China Meteorological Administration, Nanjing University of Information Science & Technology, Nanjing 210044, People's Republic of China; Department of Chemical and Biochemical Engineering, Center for Global and Regional Environmental Research, and Iowa Technology Institute, University of Iowa, Iowa City, Iowa 52242, United States*

Huanxin Zhang – *Department of Chemical and Biochemical Engineering, Center for Global and Regional Environmental Research, and Iowa Technology Institute, University of Iowa, Iowa City, Iowa 52242, United States*

Nathan Janechek – *Department of Chemical and Biochemical Engineering, Center for Global and Regional Environmental Research, and Iowa Technology Institute, University of Iowa, Iowa City, Iowa 52242, United States*

Yanyu Wang – *Shanghai Key Laboratory of Atmospheric Particle Pollution and Prevention (LAP3), Department of Environmental Science and Engineering, Institute of Atmospheric Sciences, Fudan University, Shanghai 200438, People's Republic of China; Department of Chemical and Biochemical Engineering, Center for Global and Regional Environmental Research, and Iowa Technology Institute, University of Iowa, Iowa City, Iowa 52242, United States*

Yi Wang – *Department of Chemical and Biochemical Engineering, Center for Global and Regional Environmental Research, and Iowa Technology Institute, University of Iowa, Iowa City, Iowa 52242, United States*

Lorena Castro García – *Department of Chemical and Biochemical Engineering, Center for Global and Regional Environmental Research, and Iowa Technology Institute, University of Iowa, Iowa City, Iowa 52242, United States*

G. Darrel Jenerette – *Department of Botany and Plant Sciences, University of California, Riverside, California 92521, United States*

Complete contact information is available at:
https://pubs.acs.org/10.1021/acs.est.0c06834

Notes

The authors declare no competing financial interest.

ACKNOWLEDGMENTS

This study was supported by National Natural Science Foundation of China grants (41675004 & 41975002), the National Key R&D Program of China grants (2019YFA0606802 & 2016YFA0600404), and the Postgraduate Research & Practice Innovation Program of Jiangsu Province (grant no. KYCX20_0919). G.D.J. and J.W. acknowledges the grant support from the National Science Foundation (DEB 1656062) and the Department of Agriculture in the U.S. (2019-67021-29227).

REFERENCES

(1) Seinfeld, J. H.; Pandis, S. N. *Atmospheric chemistry and physics: from air pollution to climate change*; Wiley: Hoboken, NJ, USA. 2006.

(2) Oikawa, P. Y.; Ge, C.; Wang, J.; Eberwein, J. R.; Liang, L. L.; Allsman, L. A.; Grantz, D. A.; Jenerette, G. D. Unusually high soil nitrogen oxide emissions influence air quality in a high-temperature agricultural region. *Nat. Commun.* **2015**, *6*, 8753.

(3) Rasool, Q. Z.; Zhang, R.; Lash, B.; Cohan, D. S.; Cooter, E. J.; Bash, J. O.; Lamsal, L. N. Enhanced representation of soil NO emissions in the Community Multiscale Air Quality (CMAQ) model version 5.0.2. *Geosci. Model Dev.* **2016**, *9* (9), 3177–3197.

(4) Hudman, R. C.; Moore, N. E.; Mebust, A. K.; Martin, R. V.; Russell, A. R.; Valin, L. C.; Cohen, R. C. Steps towards a mechanistic model of global soil nitric oxide emissions: implementation and space based-constraints. *Atmos. Chem. Phys.* **2012**, *12* (16), 7779–7795.

(5) Hudman, R. C.; Russell, A. R.; Valin, L. C.; Cohen, R. C. Interannual variability in soil nitric oxide emissions over the United States as viewed from space. *Atmos. Chem. Phys.* **2010**, *10* (20), 9943–9952.

(6) Jaeglé, L.; Martin, R. V.; Chance, K.; Steinberger, L.; Kurosu, T. P.; Jacob, D. J.; Modi, A. I.; Yoboué, V.; Sigha-Nkamdjou, L.; Galy-Lacaux, C. Satellite mapping of rain-induced nitric oxide emissions from soils. *J. Geophys. Res. Atmos.* **2004**, *109*, D21310.

(7) Jaegle, L.; Steinberger, L.; Martin, R. V.; Chance, K. Global partitioning of NOx sources using satellite observations: relative roles of fossil fuel combustion, biomass burning and soil emissions. *Faraday Discuss.* **2005**, *130*, 407–23.

(8) EPA: Annual Average Emissions, Air Pollutant Emission Trends Data; https://www.epa.gov/air-emissions-inventories/air-pollutant-emissions-trends-data.

(9) Jiang, Z.; McDonald, B. C.; Worden, H.; Worden, J. R.; Miyazaki, K.; Qu, Z.; Henze, D. K.; Jones, D. B. A.; Arellano, A. F.; Fischer, E. V.; Zhu, L.; Boersma, K. F. Unexpected slowdown of US pollutant emission reduction in the past decade. *Proc. Natl. Acad. Sci. U. S. A.* **2018**, *115* (20), 5099–5104.

(10) Di, Q.; Amini, H.; Shi, L.; Kloog, I.; Silvern, R.; Kelly, J.; Sabath, M. B.; Choirat, C.; Koutrakis, P.; Lyapustin, A.; Wang, Y.; Mickley, L. J.; Schwartz, J. Assessing NO2 Concentration and Model Uncertainty with High Spatiotemporal Resolution across the Contiguous United States Using Ensemble Model Averaging. *Environ. Sci. Technol.* **2020**, *54* (3), 1372–1384.

(11) Silvern, R. F.; Jacob, D. J.; Mickley, L. J.; Sulprizio, M. P.; Travis, K. R.; Marais, E. A.; Cohen, R. C.; Laughner, J. L.; Choi, S.; Joiner, J.; Lamsal, L. N. Using satellite observations of tropospheric NO2 columns to infer long-term trends in US NOx emissions: the importance of accounting for the free tropospheric NO2 background. *Atmos. Chem. Phys.* **2019**, *19* (13), 8863–8878.

(12) Jhun, I.; Coull, B. A.; Zanobetti, A.; Koutrakis, P. The impact of nitrogen oxides concentration decreases on ozone trends in the USA. *Air Qual., Atmos. Health* **2015**, *8* (3), 283–292.

(13) State of Global Air 2019; https://www.stateofglobalair.org/sites/default/files/soga_2019_report.pdf.

(14) Erickson, L. E.; Newmark, G. L.; Higgins, M. J.; Wang, Z. Nitrogen oxides and ozone in urban air: A review of 50 plus years of progress. *Environ. Prog. Sustainable Energy* **2020**, *39* (6), e13484.

(15) Parrish, D. D.; Young, L. M.; Newman, M. H.; Aikin, K. C.; Ryerson, T. B. Ozone Design Values in Southern California's Air Basins Temporal Evolution and U.S. Background Contribution. *J. Geophys. Res.* **2017**, *122*, 11166–11182.

(16) Romer, P. S.; Duffey, K. C.; Wooldridge, P. J.; Edgerton, E.; Baumann, K.; Feiner, P. A.; Miller, D. O.; Brune, W. H.; Koss, A. R.; de Gouw, J. A.; Misztal, P. K.; Goldstein, A. H.; Cohen, R. C. Effects of temperature-dependent NOx emissions on continental ozone production. *Atmos. Chem. Phys.* **2018**, *18* (4), 2601–2614.

(17) Chatani, S.; Shimadera, H.; Itahashi, S.; Yamaji, K. Comprehensive analyses of source sensitivities and apportionments of PM2.5; and ozone over Japan via multiple numerical techniques. *Atmos. Chem. Phys.* **2020**, *20* (17), 10311–10329.

(18) Li, J.; Wang, Z.; Chen, L.; Lian, L.; Li, Y.; Zhao, L.; Zhou, S.; Mao, X.; Huang, T.; Gao, H.; Ma, J. WRF-Chem simulations of ozone pollution and control strategy in petrochemical industrialized and heavily polluted Lanzhou City, Northwestern China. *Sci. Total Environ.* **2020**, *737*, 139835.

(19) Li, N.; He, Q.; Greenberg, J.; Guenther, A.; Li, J.; Cao, J.; Wang, J.; Liao, H.; Wang, Q.; Zhang, Q. Impacts of biogenic and anthropogenic emissions on summertime ozone formation in the Guanzhong Basin, China. *Atmos. Chem. Phys.* **2018**, *18* (10), 7489−7507.

(20) Pan, Y.; Zhu, Y.; Jang, J.; Wang, S.; Xing, J.; Chiang, P. C.; Zhao, X.; You, Z.; Yuan, Y. Source and sectoral contribution analysis of PM2.5 based on efficient response surface modeling technique over Pearl River Delta Region of China. *Sci. Total Environ.* **2020**, *737*, 139655.

(21) Vinken, G. C. M.; Boersma, K. F.; Maasakkers, J. D.; Adon, M.; Martin, R. V. Worldwide biogenic soil NOx emissions inferred from OMI NO2 observations. *Atmos. Chem. Phys.* **2014**, *14* (18), 10363−10381.

(22) Eberwein, J. R.; Homyak, P. M.; Carey, C. J.; Aronson, E. L.; Jenerette, G. D. Large nitrogen oxide emission pulses from desert soils and associated microbiomes. *Biogeochemistry* **2020**, *149* (3), 239−250.

(23) Yienger, J. J.; Levy, H. Empirical model of global soil-biogenic NOx emissions. *J. Geophys. Res.* **1995**, *100*, 11447−11464.

(24) Guenther, A.; Karl, T.; Harley, P.; Wiedinmyer, C.; Palmer, P. I.; Geron, C. Estimates of global terrestrial isoprene emissions using MEGAN (Model of Emissions of Gases and Aerosols from Nature). *Atmos. Chem. Phys.* **2006**, *6*, 3181−3210.

(25) Guenther, A. B.; Jiang, X.; Heald, C. L.; Sakulyanontvittaya, T.; Duhl, T.; Emmons, L. K.; Wang, X. The Model of Emissions of Gases and Aerosols from Nature version 2.1 (MEGAN2.1): an extended and updated framework for modeling biogenic emissions. *Geosci. Model Dev.* **2012**, *5* (6), 1471−1492.

(26) Steinkamp, J.; Lawrence, M. G. Improvement and evaluation of simulated global biogenic soil NO emissions in an AC-GCM. *Atmos. Chem. Phys.* **2011**, *11* (12), 6063−6082.

(27) Lin, J. T. Satellite constraint for emissions of nitrogen oxides from anthropogenic, lightning and soil sources over East China on a high-resolution grid. *Atmos. Chem. Phys.* **2012**, *12* (6), 2881−2898.

(28) Miyazaki, K.; Eskes, H.; Sudo, K.; Boersma, K. F.; Bowman, K.; Kanaya, Y. Decadal changes in global surface NOx emissions from multi-constituent satellite data assimilation. *Atmos. Chem. Phys.* **2017**, *17* (2), 807−837.

(29) Huber, D. E.; Steiner, A. L.; Kort, E. A. Daily Cropland Soil NOx Emissions Identified by TROPOMI and SMAP. *Geophys. Res. Lett.* **2020**, *47* (22), 1.

(30) Hulley, G. C.; Dousset, B.; Kahn, B. H. Rising Trends in Heatwave Metrics Across Southern California. *Earth's Future* **2020**, *8* (7), 1.

(31) Zhao, Z.; Di, P.; Chen, S.-h.; Avise, J.; Kaduwela, A.; DaMassa, J. Assessment of climate change impact over California using dynamical downscaling with a bias correction technique: method validation and analyses of summertime results. *Climate Dynamics.* **2020**, *54* (7−8), 3705−3728.

(32) Grell, G. A.; Peckham, S. E.; Schmitz, R.; McKeen, S. A.; Frost, G.; Skamarock, W. C.; Eder, B. Fully coupled "online" chemistry within the WRF model. *Atmos. Environ.* **2005**, *39* (37), 6957−6975.

(33) Grell, G. A.; Dévényi, D. A generalized approach to parameterizing convection combining ensemble and data assimilation techniques. *Geophys. Res. Lett.* **2002**, *29* (14), 38-1−38-4.

(34) Mlawer, E. J.; Taubman, S. J.; Brown, P. D.; Iacono, M. J.; Clough, S. A. Radiative transfer for inhomogeneous atmospheres: RRTM, a validated correlated-k model for the longwave. *J. Geophys. Res. Atmos.* **1997**, *102* (D14), 16663−16682.

(35) Chou, M. D.; Suarez, M. J. An efficient thermal infrared radiation parameterization for use in general circulation models. *NASA Technol. Memo.* **1994**, *104606* (3), 85.

(36) Hong, S. Y.; Noh, Y.; Dudhia, J. A new vertical diffusion package with an explicit treatment of entrainment processes. *Mon. Weather Rev.* **2006**, *134* (9), 2318.

(37) Tewari, M.; Chen, F.; Wang, W.; Dudhia, J.; LeMone, M. A.; Mitchell, K.; Ek, M.; Gayon, G.; Wegiel, J.; H, C. R. Implementation and verification of the unified NOAH land surface model in the WRF model. *20th conference on weather analysis and forecasting/16th conference on numerical weather prediction*; 2004, pp 11−15.

(38) Stockwell, W. R.; Middleton, P.; Chang, J. S.; Tang, X. The second generation regional acid deposition model chemical mechanism for regional air quality modeling. *J. Geophys. Res.* **1990**, *95* (D10), 16343.

(39) Ackermann, I. J.; Hass, H.; Memmesheimer, M.; Ebel, A.; Binkowski, F. S.; Shankar, U. Modal aerosol dynamics model for Europe: Development and first applications. *Atmos. Environ.* **1998**, *32* (17), 2981−2999.

(40) Schell, B.; Ackermann, I. J.; Hass, H.; Binkowski, F. S.; Ebel, A. Modeling the formation of secondary organic aerosol within a comprehensive air quality model system. *J. Geophys. Res. Atmos.* **2001**, *106* (D22), 28275−28293.

(41) Gelaro, R.; McCarty, W.; Suarez, M. J.; Todling, R.; Molod, A.; Takacs, L.; Randles, C.; Darmenov, A.; Bosilovich, M. G.; Reichle, R.; Wargan, K.; Coy, L.; Cullather, R.; Draper, C.; Akella, S.; Buchard, V.; Conaty, A.; da Silva, A.; Gu, W.; Kim, G. K.; Koster, R.; Lucchesi, R.; Merkova, D.; Nielsen, J. E.; Partyka, G.; Pawson, S.; Putman, W.; Rienecker, M.; Schubert, S. D.; Sienkiewicz, M.; Zhao, B. The Modern-Era Retrospective Analysis for Research and Applications, Version 2 (MERRA-2). *J. Clim.* **2017**, *30* (14), 5419−5454.

(42) Reichle, R. H.; Liu, Q.; Koster, R. D.; Draper, C. S.; Mahanama, S. P. P.; Partyka, G. S. Land Surface Precipitation in MERRA-2. *J. Clim.* **2017**, *30* (5), 1643−1664.

(43) Rodell, M.; Houser, P. R.; Jambor, U.; Gottschalck, J.; Mitchell, K.; Meng, C.-J.; Arsenault, K.; Cosgrove, B.; Radakovich, J.; Bosolovich, M.; Entin, J. K.; Walker, J. P.; Lohmann, D.; D, T. The global land data assimilation system. *Bull. Am. Meteorol. Soc.* **2004**, *85* (3), 381−394.

(44) Reid, J. S.; Hyer, E. J.; Prins, E. M.; Westphal, D. L.; Zhang, J.; J, W.; Christopher, S. A.; A, C. C.; Schmidt, C. C.; P, E. D.; A, R. K.; Hoffman, J. P. Global monitoring and forecasting of biomass-burning smoke: Description of and lessons from the fire Locating and Modeling of Burning Emissions (FLAMBE) program. *IEEE J. Sel. Top. Appl. Earth Obs. Remote Sens.* **2009**, *2*, 144−162.

(45) Wang, J.; Ge, C.; Yang, Z.; Hyer, E. J.; Reid, J. S.; Chew, B.-N.; Mahmud, M.; Zhang, Y.; Zhang, M. Mesoscale modeling of smoke transport over the Southeast Asian Maritime Continent: Interplay of sea breeze, trade wind, typhoon, and topography. *Atmos. Res.* **2013**, *122*, 486−503.

(46) Ge, C.; Wang, J.; Reid, J. S. Mesoscale modeling of smoke transport over the Southeast Asian Maritime Continent: coupling of smoke direct radiative effect below and above the low-level clouds. *Atmos. Chem. Phys.* **2014**, *14* (1), 159−174.

(47) Tomich, T. P.; Six, J.; Liptzin, D.; Rosenstock, T. S. Nitrogen fertilizer use in California: Assessing the data, trends and a way forward. *Calif. Agric.* **2013**, *67* (1), 68−79.

(48) TROPOMI ATBD of the total and tropospheric NO2 data products; https://sentinel.esa.int/documents/247904/2476257/Sentinel-5P-TROPOMI-ATBD-NO2-data-products.

(49) van Geffen, J.; Boersma, K. F.; Eskes, H.; Sneep, M.; ter Linden, M.; Zara, M.; Veefkind, J. P. S5P TROPOMI NO2 slant column retrieval: method, stability, uncertainties and comparisons with OMI. *Atmos. Meas. Tech.* **2020**, *13* (3), 1315−1335.

(50) Bauwens, M.; Compernolle, S.; Stavrakou, T.; Muller, J. F.; van Gent, J.; Eskes, H.; Levelt, P. F.; van der, A. R.; Veefkind, J. P.; Vlietinck, J.; Yu, H.; Zehner, C. Impact of coronavirus outbreak on NO2 pollution assessed using TROPOMI and OMI observations. *Geophys. Res. Lett.* **2020**, e2020GL087978.

(51) SMAP L4 9 km EASE-Grid Surface and Root Zone Soil Moisture Geophysical Data, Version 3.

(52) NASA Global Precipitation Measurement (GPM) Integrated Multi-satellitE Retrievals for GPM (IMERG); https://docserver.gesdisc.eosdis.nasa.gov/public/project/GPM/IMERG_ATBD_V06.pdf.

(53) S5P Mission Performance Centre Nitrogen Dioxide [L2__NO2___] Readme; 2020−11−26 Released; https://sentinels.copernicus.eu/documents/247904/3541451/Sentinel-5P-Nitrogen-Dioxide-Level-2-Product-Readme-File.

(54) OMSO2 README File v1.1.1 Released Feb 26, 2008 Updated: August 18, 2008; https://so2.gsfc.nasa.gov/Documentation/OMSO2Readme_V111.pdf.

(55) Zyrichidou, I.; Koukouli, M. E.; Balis, D.; Markakis, K.; Poupkou, A.; Katragkou, E.; Kioutsioukis, I.; Melas, D.; Boersma, K. F.; van Roozendael, M. Identification of surface NOx emission sources on a regional scale using OMI NO2. *Atmos. Environ.* **2015**, *101*, 82−93.

(56) Beirle, S.; Borger, C.; Dorner, S.; Li, A.; Hu, Z.; Liu, F.; Wang, Y.; Wagner, T. Pinpointing nitrogen oxide emissions from space. *Sci. Adv.* **2019**, *5*, eaax9800.

(57) Goldberg, D. L.; Lu, Z.; Streets, D. G.; de Foy, B.; Griffin, D.; McLinden, C. A.; Lamsal, L. N.; Krotkov, N. A.; Eskes, H. Enhanced Capabilities of TROPOMI NO2: Estimating NOx from North American Cities and Power Plants. *Environ. Sci. Technol.* **2019**, *53* (21), 12594−12601.

(58) Fang, Y.; Fiore, A. M.; Horowitz, L. W.; Levy, H.; Hu, Y.; Russell, A. G. Sensitivity of the NOy budget over the United States to anthropogenic and lightning NOx in summer. *J. Geophys. Res.* **2010**, *115*, D18312.

(59) Peterson, H. S.; Williams, E. R.; Blakeslee, R. J.; Vant-Hull, B.; Buechler, D. E.; Cummins, K. L.; Koshak, W. J. Variability of CONUS Lightning in 2003−12 and Associated Impacts. *J. APPL. METEOROL. CLIM.* **2015**, *54* (1), 15−41.

(60) Kang, D.; Mathur, R.; Pouliot, G. A.; Gilliam, R. C.; Wong, D. C. Significant ground-level ozone attributed to lightning-induced nitrogen oxides during summertime over the Mountain West States. *NPJ. Clim Atmos Sci.* **2020**, *3*, 6.

(61) Almaraz, M.; Bai, E.; Wang, C.; Trousdell, J.; Conley, S.; Faloona, I.; Houlton, B. Z. Agriculture is a major source of NOx pollution in California. *Sci. Adv.* **2018**, *4*, eaao3477.

(62) Jacob, D. J.; Backwin, P. S. *Cycling of NOx in tropical forest canopies and its implications for the global source of biogenic NOx to the atmosphere*; American Society of Microbiology: 1991.

(63) Delaria, E. R.; Place, B. K.; Liu, A. X.; Cohen, R. C. Laboratory measurements of stomatal NO2 deposition to native California trees and the role of forests in the NOx cycle. *Atmos. Chem. Phys.* **2020**, *20* (22), 14023−14041.

(64) Anderson, D. C.; Loughner, C. P.; Diskin, G.; Weinheimer, A.; Canty, T. P.; Salawitch, R. J.; Worden, H. M.; Fried, A.; Mikoviny, T.; Wisthaler, A.; Dickerson, R. R. Measured and modeled CO and NOy in DISCOVER-AQ: An evaluation of emissions and chemistry over the eastern US. *Atmos. Environ.* **2014**, *96*, 78−87.

(65) Travis, K. R.; Jacob, D. J.; Fisher, J. A.; Kim, P. S.; Marais, E. A.; Zhu, L.; Yu, K.; Miller, C. C.; Yantosca, R. M.; Sulprizio, M. P.; Thompson, A. M.; Wennberg, P. O.; Crounse, J. D.; St Clair, J. M.; Cohen, R. C.; Laughner, J. L.; Dibb, J. E.; Hall, S. R.; Ullmann, K.; Wolfe, G. M.; Pollack, I. B.; Peischl, J.; Neuman, J. A.; Zhou, X. Why do Models Overestimate Surface Ozone in the Southeastern United States? *Atmos. Chem. Phys.* **2016**, *16* (21), 13561−13577.

(66) Jaeglé, L.; Shah, V.; Thornton, J. A.; Lopez-Hilfiker, F. D.; Lee, B. H.; McDuffie, E. E.; Fibiger, D.; Brown, S. S.; Veres, P.; Sparks, T. L.; Ebben, C. J.; Wooldridge, P. J.; Kenagy, H. S.; Cohen, R. C.; Weinheimer, A. J.; Campos, T. L.; Montzka, D. D.; Digangi, J. P.; Wolfe, G. M.; Hanisco, T.; Schroder, J. C.; Campuzano-Jost, P.; Day, D. A.; Jimenez, J. L.; Sullivan, A. P.; Guo, H.; Weber, R. J. Nitrogen Oxides Emissions, Chemistry, Deposition, and Export Over the Northeast United States During the WINTER Aircraft Campaign. *J. Geophys. Res.: Atmos.* **2018**, *123* (21), 12,368−12,393.

(67) McDonald, B. C.; McKeen, S. A.; Cui, Y. Y.; Ahmadov, R.; Kim, S. W.; Frost, G. J.; Pollack, I. B.; Peischl, J.; Ryerson, T. B.; Holloway, J. S.; Graus, M.; Warneke, C.; Gilman, J. B.; de Gouw, J. A.; Kaiser, J.; Keutsch, F. N.; Hanisco, T. F.; Wolfe, G. M.; Trainer, M. Modeling Ozone in the Eastern U.S. using a Fuel-Based Mobile Source Emissions Inventory. *Environ. Sci. Technol.* **2018**, *52* (13), 7360−7370.

(68) Lin, L.-F.; Ebtehaj, A. M.; Wang, J. F.; Bras, R. L. Soil moisture background error covariance and data assimilation in a coupled land-atmosphere model. *Water Resour. Res.* **2017**, *53*, 1309−1335.

(69) Quarterly Validation Report of the Copernicus Sentinel-5 Precursor Operational Data Products #05: April 2018; http://www.tropomi.eu/sites/default/files/files/publicS5P-MPC-IASB-ROCVR-05.0.1-20191217_FINAL.pdf.

(70) Griffin, D.; Zhao, X.; McLinden, C. A.; Boersma, F.; Bourassa, A.; Dammers, E.; Degenstein, D.; Eskes, H.; Fehr, L.; Fioletov, V.; Hayden, K.; Kharol, S. K.; Li, S. M.; Makar, P.; Martin, R. V.; Mihele, C.; Mittermeier, R. L.; Krotkov, N.; Sneep, M.; Lamsal, L. N.; Linden, M. t.; Geffen, J. v.; Veefkind, P.; Wolde, M. High-Resolution Mapping of Nitrogen Dioxide With TROPOMI: First Results and Validation Over the Canadian Oil Sands. *Geophys. Res. Lett.* **2019**, *46* (2), 1049−1060.

(71) Judd, L. M.; Al-Saadi, J. A.; Janz, S. J.; Kowalewski, M. G.; Pierce, R. B.; Szykman, J. J.; Valin, L. C.; Swap, R.; Cede, A.; Mueller, M.; Tiefengraber, M.; Abuhassan, N.; Williams, D. Evaluating the impact of spatial resolution on tropospheric NO2 column comparisons within urban areas using high-resolution airborne data. *Atmos. Meas. Tech.* **2019**, *12* (11), 6091−6111.

(72) Zhao, X.; Griffin, D.; Fioletov, V.; McLinden, C.; Cede, A.; Tiefengraber, M.; Müller, M.; Bognar, K.; Strong, K.; Boersma, F.; Eskes, H.; Davies, J.; Ogyu, A.; Lee, S. C. Assessment of the quality of TROPOMI high-spatial-resolution NO2 data products in the Greater Toronto Area. *Atmos. Meas. Tech.* **2020**, *13* (4), 2131−2159.